Highly Reversible Aqueous Zinc-ion Batteries *via* Multifunctional Hydrogen-Bond-rich Dulcitol at Lower Temperature

Ya He, [#, a] *Zhuo Chen,* [#, a] *Junrun Feng,* [*, a] *Jian Wang,* [a] *Lun Zhang,* [b] *Hao Gu,* [b] *Lin Sheng,* [c] *Pengfei Yao,* [a] *Feng Ryan Wang,* [b] *Zhangxiang Hao*[*, a]

a School of Science, School of Chip Industry, Hubei University of Technology, Wuhan, Hubei 430068, China

b Materials and Catalysis Laboratory, Department of Chemical Engineering, University College London, London WC1E 7JE, United Kingdom

c School of Mechanical and Electronic Engineering, Suzhou University, Suzhou, Anhui 234000, China

# authors contributed equally to the paper

*Corresponding author. E-mail: haozx@hbut.edu.cn; fengjunrun@hbut.edu.cn

Keywords: aqueous zinc-ions batteries, dulcitol, Zn deposition, low temperatures, hydrogen-bonding-rich

ABSTRACT

Aqueous zinc-ion batteries (AZIBs) are considered one of the most promising next-generation energy storage devices due to cost-effectiveness and high safety. However, the uncontrolled dendrite growth and the intolerance against low temperatures hinder the application of AZIBs. Herein, hydrogen-bonding-rich dulcitol (DOL) was introduced into the $ZnSO_4$, which reshaped the hydrogen-bond network in the electrolyte and optimised the solvation sheath structure, effectively reduces the amount of active water molecules and inhibiting hydrogen evolution and the parasitic reaction at the zinc anode. In addition, higher adsorption energy DOL preferentially adsorbs on the surface of the zinc anode, guiding the uniform deposition of Zn^{2+} and inhibiting the formation of dendrites. DOL also enhances the interaction between free and free water and improves the resistance to freeze of the electrolyte. Consequently, the Zn//Zn symmetric cells assembled with DOL was extremely stable cycled for 2000 h at 2 mA cm^{-2}. The $NH_4V_4O_{10}$ (NVO)//Zn full cell showed more excellent specific capacity of 183.07 mAh g^{-1} after 800 cycles. Even at the low temperature of -10 °C, the cell still maintains 155.95 mAh g^{-1} capacity after 600 cycles. This work provides a new strategy for the subsequent study of AZIBs with high stability at low temperatures.

1. Introduction

Energy storage devices are pivotal technologies for achieving the global goals of "carbon peaking and carbon neutrality". Lithium-ion (LIBs) and sodium-ion (SIBs) batteries pose inherent or explosive safety risks due to traditional organic electrolytes.[1–4] Aqueous zinc-ion batteries (AZIBs) have emerged as promising candidates for sustainable energy storage due to their multiple advantages. They offer impressive theoretical specific capacities and energy densities (820 mAh g^{-1}, 5855 mAh cm^{-2}), while maintaining high safety standards and environmental friendliness. The zinc metal anode exhibits a suitable redox potential (-0.76 V *vs*. Standard Hydrogen Electrode) and benefits from high earth abundance, which significantly reduces manufacturing costs. These characteristics make AZIBs an attractive alternative to conventional lithium-ion batteries for large-scale energy storage applications.[5–7] However, several critical challenges impede their practical implementation. The active water molecules in aqueous electrolytes can trigger hydrogen evolution reaction (HER), compromising operational safety. Moreover, parasitic reactions between zinc metal and the electrolyte result in the formation of an inert $Zn_4SO_4(OH)_6{\cdot}xH_2O$ (ZHS) interface layer, which promotes dendrite formation and potentially leads to internal short circuits.[8,9] The aqueous nature of the electrolyte also limits low-temperature operation, as it tends to freeze below 0°C, significantly restricting the application scenarios of AZIBs. These issues have hindered the further development of AZIBs. Therefore, an urgent need exists for electrolyte additives to stabilize the zinc anode and ensure proper operation even at low temperatures.[10–12]

To address these challenges, extensive research efforts have been devoted to understanding and mitigating zinc anode degradation mechanisms. Various strategies have been developed, primarily focusing on two aspects, which are zinc anode surface engineering and electrolyte optimization (Table S1). These approaches aim to simultaneously suppress the HER and inhibit dendrite formation, thereby enhancing the stability of zinc anodes.[13–16] Among various strategies, electrolyte modification stands out as a cost-effective and operationally simple approach. Current research has explored diverse additives with different functional mechanisms. For instance, Mai *et al.* demonstrated that glucose, as an economical additive, could effectively modulate both the Zn^{2+} solvation structure and the zinc anode-electrolyte interface in $ZnSO_4$ electrolytes. By displacing one H_2O molecule from the Zn $[(H_2O)_6]^{2+}$ complex, glucose successfully suppressed parasitic reactions between active water and the zinc anode. This modification enabled remarkable stability in Zn//Zn symmetric cells, achieving stable cycling for

2000 h at 1 mA cm^{-2} and 1 mAh cm^{-2}.[17] In another approach, Chen *et al.* investigated the combined effects of diethyl ether and ethylene glycol (EG/30% and Et_2O/1%) on electrolyte properties. Their strategy focused on modifying the water molecules' hydrogen bonding network to lower the electrolyte's freezing point. However, this approach showed limited success. While it extended the operational temperature range, the overall battery performance remained suboptimal. In MnO_2//Zn full cells at -10°C, capacity retention was only about 55 % after 400 cycles at 3 A g^{-1}, and even at room temperature, capacity degradation reached nearly 50 % within a short period.[18] Current electrolyte additives exhibit notable limitations in their functionality. The first type effectively modifies the solvation structure, enabling stable battery cycling but fails to address low-temperature operation issues. The second type improves low-temperature performance but, due to their inherent properties, adversely affects Zn^{2+} ion transport kinetics. These limitations highlight the urgent need for developing novel multifunctional electrolyte additives that can simultaneously optimize low-temperature performance while maintaining highly reversible and stable zinc anode operation.[19–21]

Among many organic substances, hydroxyl-rich alcohols have been found to be promising electrolyte additives due to their unique properties. Their polyhydroxyl nature not only contributes to hydrophilicity and rich hydrogen bonding networks but also effectively regulates free water content and significantly reduces the electrolyte's freezing point. These multifunctional characteristics make them particularly suitable for electrolyte optimization. Herein, we introduced 1,4-dioxane-2,5-diol (DOL) as a multifunctional additive into 2 M $ZnSO_4$ electrolyte to achieve highly reversible AZIBs. DOL with hydroxyl-rich structure enables multiple beneficial modifications to the electrolyte system. By remodeling the hydrogen-bonding network and partially replacing H_2O molecules in the Zn $[(H_2O)_6]^{2+}$ complex, DOL effectively enhances the Zn^{2+} transference number. Additionally, it reduces the content of active water in the electrolyte, thereby suppressing parasitic reactions at the zinc anode interface. The polyhydroxyl structure of DOL facilitates stronger surface adsorption compared to H_2O molecules, promoting homogeneous zinc deposition and effectively suppressing dendrite growth. This characteristic significantly enhanced the cycle life of the zinc anode (Figure 1a). Attributing to the above advantages, the Zn//Zn symmetric cell with DOL additives can be stably cycled for 2000 h at 2 mA cm^{-2} and 1 mAh cm^{-2}. Moreover, when evaluated in NVO//Zn full cells at a current density of 1 A g^{-1}, the system maintained a high capacity of 183.07 mAh g^{-1} with 63% capacity retention after 800 cycles. Furthermore, the hydrogen bonding interactions between DOL's hydroxyl groups and water molecules effectively reduce the free water content in the electrolyte, thereby enhancing the system's low-temperature tolerance. This improved freezing resistance was demonstrated in NVO//Zn full cells, which maintained a high capacity of 155.95 mAh g^{-1} after 600 cycles at -10 °C.

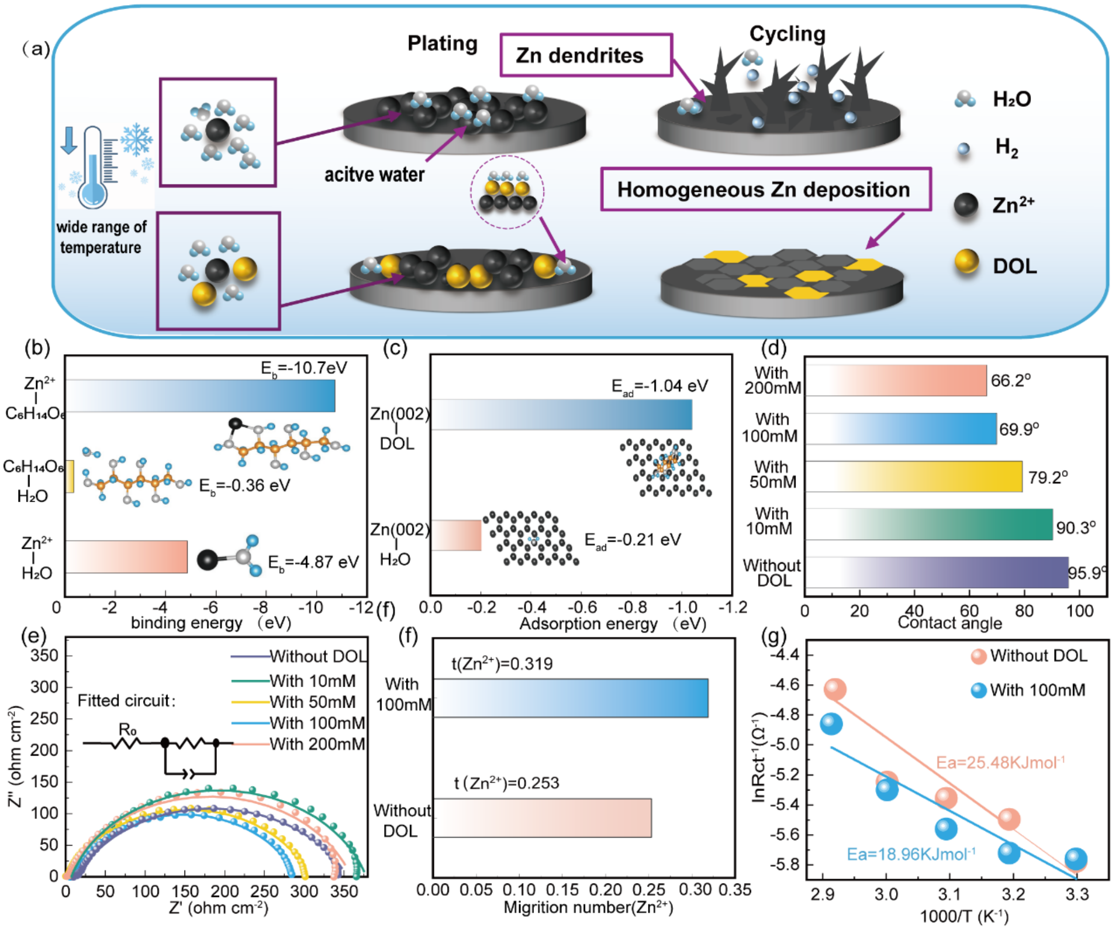

Figure 1. (a) Schematic diagram of the mechanism without and with DOL additives. (b) Binding energy values for H_2O, DOL with Zn^{2+} and H_2O with DOL. (c) Adsorption energy of H_2O and DOL on Zn (002) crystal plane. (d) Comparison of contact angles of various electrolytes. (e) Nyquist plots of the Zn//Zn symmetric cell with different amounts of DOL. The insert figure is fitted circuit. (f) Zn^{2+} transfer number in the different electrolytes. (g) Corresponding to the activation energy of the desolventised sheath of two electrolytes.

2. Results and Discussion

To elucidate the interaction mechanism, Density Functional Theory (DFT) calculations were performed to evaluate the binding energies in the 2M $ZnSO_4$ electrolyte with DOL additives. The computational results revealed that DOL exhibits remarkably strong binding with Zn (-10.72 eV), which is more than twice the binding energy between Zn and water molecules (-4.87 eV) (Figure 1b). This enhanced binding affinity enables DOL to effectively reconstruct the Zn^{2+} solvation sheath, reducing active water content and suppressing both side reactions and dendrite formation at the electrode-electrolyte interface. To understand the intrinsic mechanism of DOL-induced Zn deposition behavior, DFT calculations were performed to evaluate the interaction between DOL, H_2O, and different Zn crystal planes. The calculations revealed that DOL exhibits stronger adsorption energies than H_2O on all Zn crystal faces, indicating that DOL molecules preferentially adsorb on the Zn surface over water molecules. Notably, the adsorption energies of DOL on Zn(100), Zn(101), and Zn(002) were -1.59, -1.53, and -1.04 eV, respectively. This differential adsorption behavior suggests that DOL would selectively adsorb on (100) and (101) planes, hindering Zn^{2+} deposition on these surfaces. Consequently, Zn^{2+} tends to deposit on the more exposed (002) plane. Due to the lowest surface energy of the Zn(002) crystal plane, this oriented deposition behavior not only promotes uniform Zn plating but also contributes to enhanced cycling stability, as demonstrated by our subsequent electrochemical performance tests (Figure 1C, S1).[22,23]

A systematic investigation was conducted to optimize the DOL concentration in 2 M $ZnSO_4$ electrolyte (Figure S2). The DOL molecule, featuring 6 hydroxyl groups, significantly enhances the wettability of the originally hydrophobic $ZnSO_4$ electrolyte. Contact angle measurements reveal that the addition of DOL, which is highly soluble in the aqueous electrolyte, effectively enhances electrolyte wettability. The contact angles systematically decrease from 95.9° (without DOL) to 69.9° (100mM DOL) and 66.2°(200mM DOL). Although 200mM DOL shows slightly lower contact angles, the optimal concentration of 100mM DOL was determined through comprehensive evaluation of multiple parameters, including electrochemical performance tests, surface characterizations, and stability studies (Figure 1d, S3). [24] This concentration provides the best balance of various beneficial effects, as demonstrated by our systematic characterization results. DOL demonstrates enhanced affinity towards the zinc anode, preferentially adsorbing on the zinc surface compared to water molecules, thereby promoting homogeneous zinc deposition while reducing the concentration of reactive water molecules.[25] To further investigate the impact of DOL on charge transfer kinetics, electrochemical impedance spectroscopy (EIS) was conducted using Zn//Zn symmetric cells. The Nyquist plots exhibited characteristic charge-transfer semicircles, with DOL addition maintaining the same interfacial processes while significantly reducing the charge transfer resistance. Specifically, the impedance decreased from 341.9 Ω (pristine electrolyte) to 282.99 Ω upon DOL addition, with 100 mM DOL showing the lowest impedance value (Figure 1e).[26] In addition, The electrochemical reversibility of the DOL-modified electrolyte was evaluated through rate capability tests in Zn//Zn symmetric cells. The system maintained stable voltage profiles during stepwise current density variations from 0.5 to 2 mA cm^{-2} and back to 0.5 mA cm^{-2} (Figure S4), further confirming DOL's role in facilitating uniform zinc deposition.[27] Based on these comprehensive results, 100 mM was established as the optimal DOL concentration for subsequent investigations.

For further verification, the impedance of the Zn//Zn symmetric cells assembled with different electrolytes was measured before and after cycling and the Zn^{2+} transfer number was calculated (Eq S1). The results showed that the Zn^{2+} transfer number was higher with the addition of DOL than without DOL (0.319 *vs.* 0.253) (Figure 1f, S5), which indicated that the protective layer formed by DOL promoted the transfer of ions, reduced the accumulation of by-products, and guided the homogeneous deposition of Zn^{2+}. To elucidate how DOL modifies the Zn^{2+} solvation structure, we investigated the interfacial charge transfer kinetics through temperature-dependent EIS measurements. The activation energies were calculated using the Arrhenius equation (Eq. S2) based on impedance data collected from Zn//Zn symmetric cells at temperatures ranging from 30 to 70°C. The results reveal that the addition of 100 mM DOL reduces the activation energy from 25.48 kJ mol^{-1} to 18.96 kJ mol^{-1} (Figure 1g, S6). This significant decrease in activation energy suggests a weakened Zn^{2+}-solvent interaction and modified solvation shell structure, which facilitates the desolvation process during Zn^{2+} transport.[28] Through the above series of experiments, it is speculated that the addition of DOL will reconstruct the solvated structure, and DOL will replace part of H_2O, reducing the amount of active water. In addition, the steric hindrance generated by DOL makes the solvated structure loose, and Zn is more likely to dissolve and migrate, and eventually deposit on the electrode surface after separating from solvent molecules.

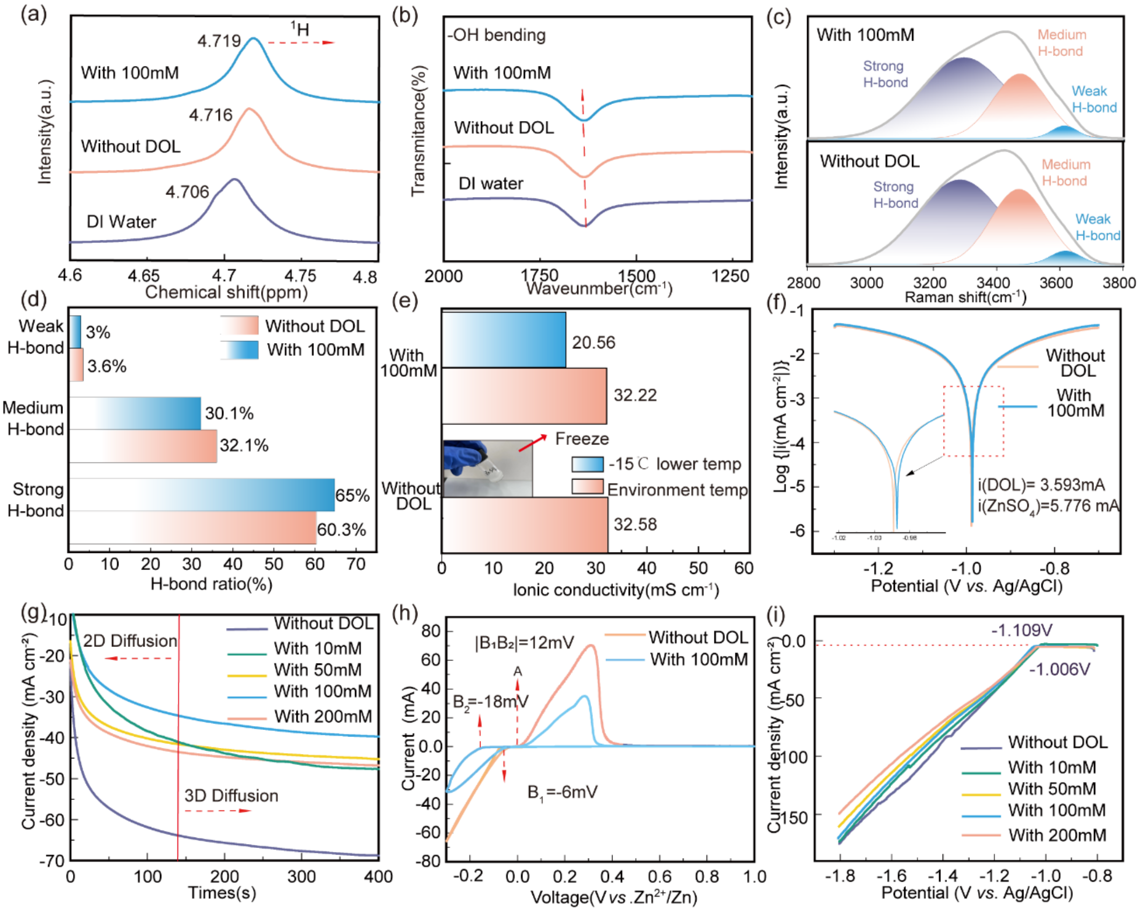

Figure 2. Characterization of various electrolytes. (a) ^{1}NMR spectrum of H_2O, $ZnSO_4$, and with 100mM DOL. (b) FT-IR spectrum of O-H blending in H_2O, $ZnSO_4$ and with 100 mM DOL. (c) Fitted Raman spectrum of strong, medium, and weak hydrogen bonds vibration region. (d) Comparison of strong, medium, and weak hydrogen bonding content. (e) Ionic conductivity of different levels of DOL at environment temperatures (25 °C) and -10 °C. (f) Tafel curves of different electrolytes were tested for the three-electrode system at 1 mV S^{-1}. (g) CA curves of $ZnSO_4$ and with 100 mM DOL at -150 mV. (h) CV curves of Zn//Ti asymmetric cells $ZnSO_4$ and with 100 mM DOL at 10 mV s^{-1}. (i) LSV curves at 1 mV S^{-1} for different electrolytes.

After the above series of electrochemical tests, changes in the chemical environment at 100 mM DOL were explored using a series of spectral analyses. The ^{1}H NMR spectra revealed an upfield shift from 4.716 ppm to 4.719 ppm upon DOL addition (Figure 2a), indicating enhanced electron shielding of H_2O molecules and weakened Zn^{2+}-H_2O interactions, thus demonstrating DOL's role in modifying the solvation sheath structure.[29,30] This observation was further supported by Fourier transform infrared spectroscopy (FT-IR), which showed slight increases in O-H vibrational frequencies around 1625 and 3200 cm^{-1}, accompanied by a decrease in v(SO_4^{2-}) intensity around 1100 cm^{-1} (Figure 2b, S7), confirming DOL's interaction with both water molecules and SO_4^{2-} species.[31–33] Raman spectroscopy was employed to further analyze the solvated sheath of $Zn[(H_2O)_6]^{2+}$. The O-H vibration frequencies at 3200, 3400, and 3600 cm^{-1} were assigned to strong, medium, and weak hydrogen bonding, respectively. As shown in Figure 2c, quantitative analysis revealed that the proportion of strong hydrogen bonding increased significantly from 60.3 % to 65 %, while the weak hydrogen bonding content decreased (3 %) (Figure 2d). These results indicate that DOL effectively converts active water molecules in the solvation shell to less reactive bulk water, simultaneously restructuring the solvation environment and suppressing the HER.[34]

Ionic conductivity is a critical parameter for electrolyte performance. EIS measurements were conducted to evaluate the ionic conductivity of electrolytes with varying DOL concentrations. The results revealed a slight decrease in ionic conductivity with increasing DOL content, attributed to the elevated kinematic viscosity of the modified electrolytes (Figure S8, S9). Notably, despite this minor conductivity reduction, an unexpected beneficial effect was observed at low temperatures. The electrolyte containing 100 mM DOL maintained a substantial ionic conductivity of 20.86 mS cm^{-1} at -10 °C (Eq. S3), even when the pristine $ZnSO_4$ electrolyte had frozen (Figure 2e). This enhanced antifreeze capability of the DOL-modified electrolyte enables AZIB operation at low temperatures, as demonstrated in subsequent low-temperature performance evaluations.[35]

The electrochemical performance enhancement of DOL-modified electrolyte was systematically evaluated through multiple electrochemical techniques. Linear polarization (Tafel) analysis demonstrated improved anti-corrosion properties, with the corrosion current density decreasing from 5.766 to 3.593 mA cm^{-2} and the corrosion potential shifting positively from -0.989 to -0.986 V upon DOL addition (Figure 2f). This enhanced corrosion resistance was further validated through XRD analysis of Zn electrodes after electrolyte immersion, showing significantly reduced zinc hydroxide sulfate (ZHS) by-product formation in the DOL-modified electrolyte, with minimal by-product peaks observed at the optimal DOL concentration (Figure S10) [18] Chronoamperometry (CA) measurements at -0.15 V revealed distinct Zn^{2+} diffusion behaviors. The pristine electrolyte exhibited rapid current density decay within 75 s, followed by continuous deterioration over 400 s. In contrast, the 100 mM DOL-modified electrolyte showed gradual current density reduction during the initial 100 s before stabilizing, indicating a transition from 2D to 3D diffusion mode (Figure 2g). This behavior confirms improved zinc deposition kinetics and suppresses dendrite formation.[36,37] Cyclic voltammetry (CV) analysis of Zn//Ti asymmetric cells revealed the impact of DOL on Zn^{2+} nucleation behavior. The pristine electrolyte showed a small nucleation overpotential (6 mV), indicating unfavorably large initial nuclei formation. In contrast, the 100 mM DOL-modified electrolyte exhibited an increased overpotential (18 mV) (Figure 2h), suggesting reduced nucleus size that promotes uniform zinc deposition.[38,39] Meanwhile, the Zn//Ti cell was assembled and discharged at 2 mA cm^{-2}, 1 mAh cm^{-2} for half hour to quantitatively test the nucleation overpotential. The 100 mM DOL-modified electrolyte exhibited a remarkably low nucleation overpotential of 55.6 mV, significantly outperforming other electrolyte formulations (Figure S11).[23] This result corroborates the CV findings, further confirming DOL's role in enhancing zinc deposition kinetics.[40] To quantitatively evaluate the impact of DOL on side reactions, particularly HER, we conducted linear sweep voltammetry (LSV) measurements at 1 mV s^{-1} using a three-electrode system. The LSV curves demonstrate that incorporating 100 mM DOL shifts the HER onset potential negatively from -1.006 V to -1.109 V (Figure 2i). This 103 mV increase in overpotential indicates a higher energy barrier for water reduction, confirming that DOL effectively suppresses the HER side reaction. This suppression can be attributed to the reduced water activity in the electrolyte due to DOL's coordination with water molecules.

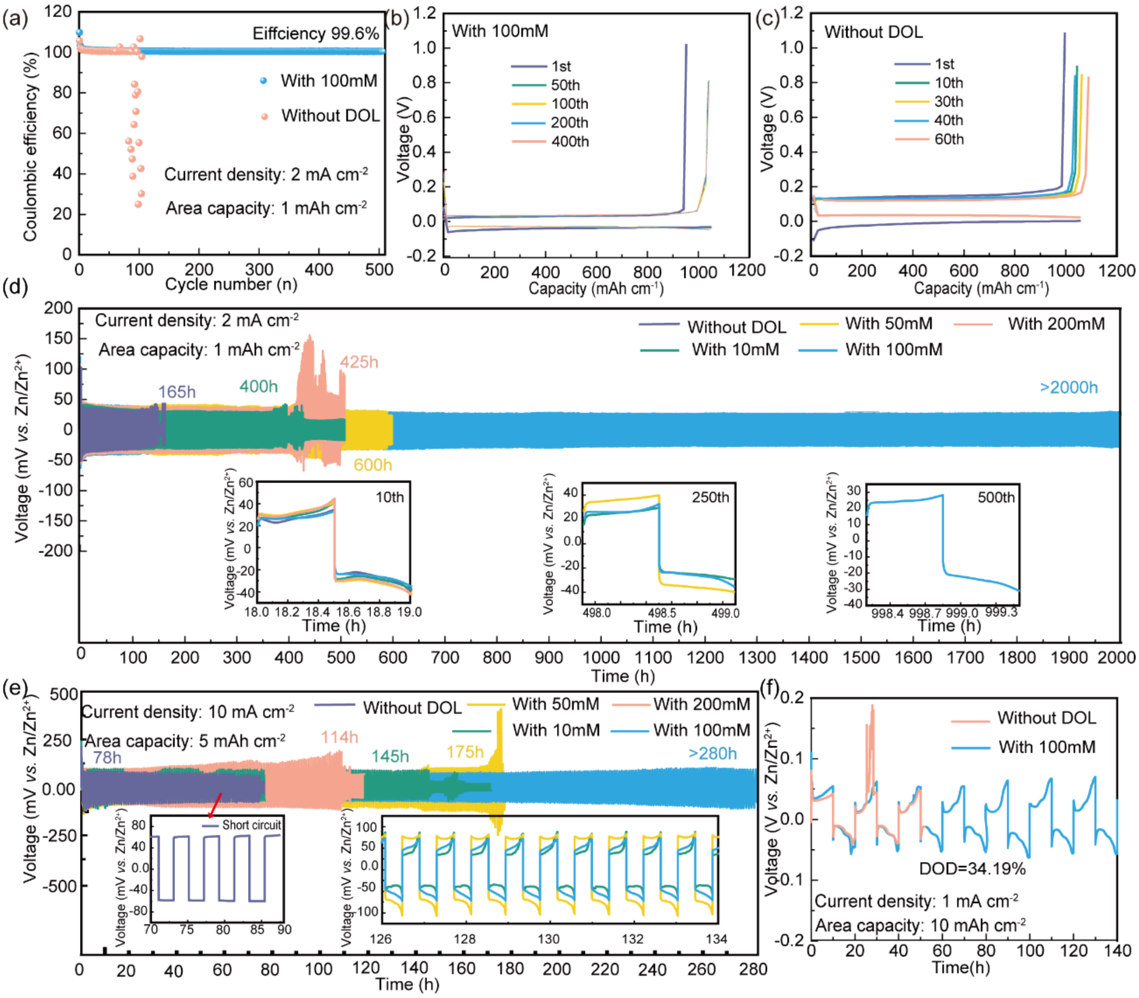

Figure 3. Electrochemical behavior of cells assembled with $ZnSO_4$ and DOL modified electrolytes. (a) CE curves of Zn//Cu asymmetric cells at a current density of 2 mA cm^{-2} and an area capacity of 1 mAh cm^{-2}. Corresponding to the voltage profile of Zn//Cu cell (b) with 100 mM DOL, and (c) $ZnSO_4$ electrolytes. Long-cycle performance of Zn//Zn symmetric cells in various electrolytes at current densities of d) 2 mA cm^{-2} and area capacity of 1 mAh cm^{-2}, and e) 10 mA cm^{-2} and area capacity of 5 mAh cm^{-2} cycles. The inserted figure shows the comparison of potentials with various electrolytes at different numbers of cycles. f) The DOD of Zn anode with different electrolytes.

The impact of DOL on Zn plating/stripping behavior was evaluated using Zn//Cu cells to determine coulombic efficiency (CE), a critical indicator of long-term cycling stability. The electrolyte containing 100 mM DOL maintained a remarkably stable CE of 99.6 % with a cut-off voltage of 0.8 V, whereas the pristine electrolyte exhibited only 99.4 % CE briefly before showing significant instability after 70 cycles, leading to premature cell failure. Voltage profiles revealed consistently lower hysteresis in DOL-modified electrolytes throughout cycling, with more stable zinc plating/stripping curves compared to the DOL-free electrolyte (Figure 3b, 3c).[41,42] The stability enhancement was further validated through Zn//Zn symmetrical cell tests under various conditions. At 2 mA cm^{-2} with 1 mAh cm^{-2}, the DOL-modified electrolyte demonstrated stable cycling for 2000 h, while the pristine electrolyte experienced short-circuit failure around 160 h. Notably, the polarization potential analysis revealed that although DOL-containing cells showed higher initial polarization (~20 h) due to electrode surface activation, the potential gradually decreased to approximately 25 mV at 1000 h (Figure 3d). Under more demanding conditions (10 mA cm^{-2}, 3 mAh cm^{-2}), the DOL-modified electrolyte maintained stable cycling beyond 300 h, whereas the DOL-free cells failed around 60 h (Figure S12). Similarly, at 10 mA cm^{-2} with 5 mAh cm^{-2}, the DOL-modified system achieved stable cycling for over 280 h, contrasting with the pristine electrolyte's failure around 80h, as evidenced by voltage profile comparisons at different time intervals (Figure 3e). Comparative studies with DOL isomers (Mannitol and Sorbitol) at 10 mA cm^{-2} and 5 mAh cm^{-2} demonstrated the superior performance of DOL-modified electrolytes (Figure S13).[43,44] Furthermore, ultra-thin (30 μm) Zn//Zn symmetric cells with DOL-modified electrolyte maintained stable cycling at a high depth of discharge (DOD) of 34.19% (Figure 3f).[45] These comprehensive results consistently demonstrate DOL's effectiveness in enhancing electrode stability and facilitating reversible Zn^{2+} insertion/extraction processes..[46–49]

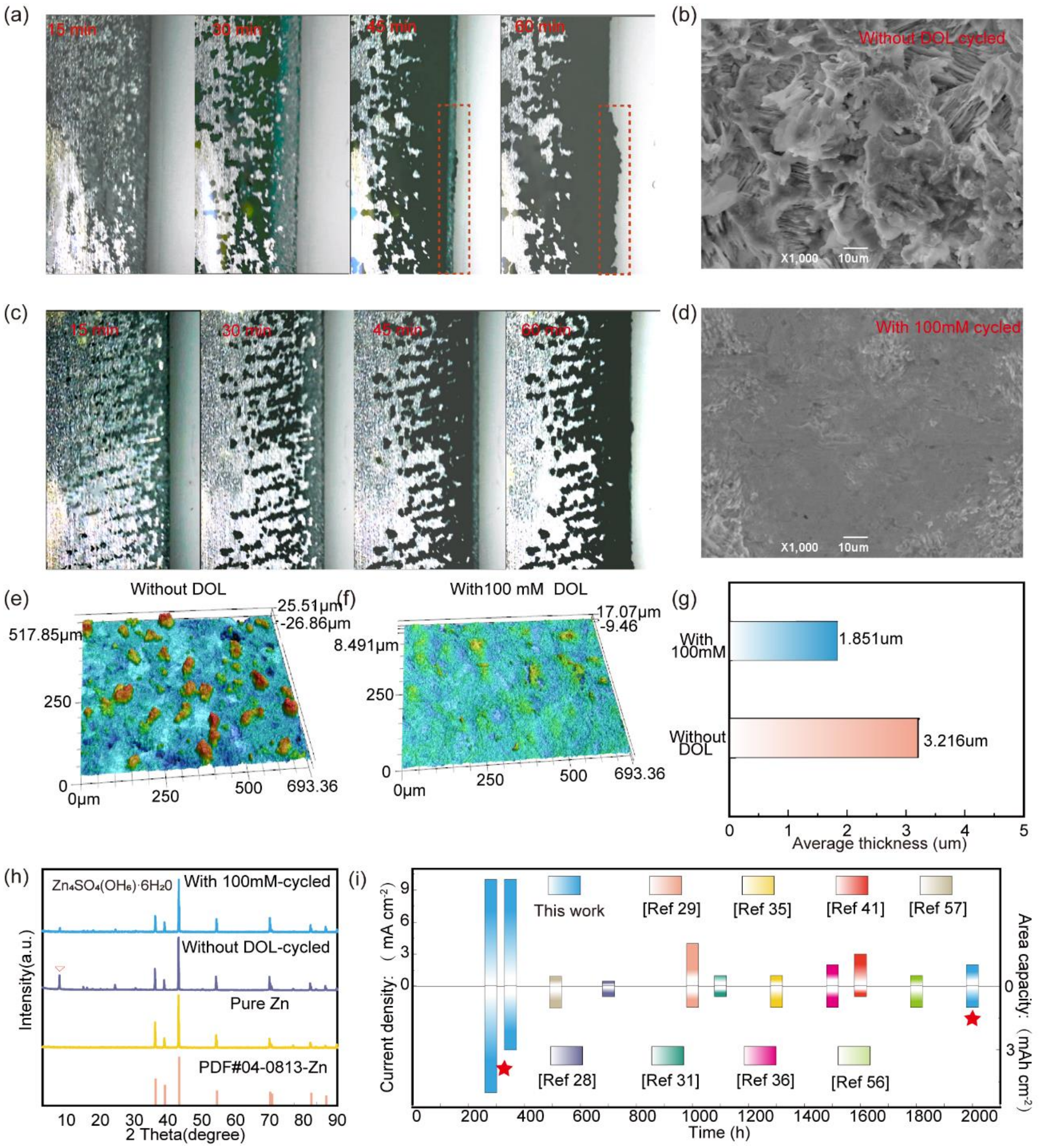

Figure 4. Zn deposition morphology with different electrolytes. *In-situ* optical microscope and SEM images of different electrolytes at 1h. (a) and (b) without DOL. (c) and (d) with 100mM DOL. AFM images after cycling of different electrolytes, (b) without DOL. (d) with 100mM DOL. (e) CLSM 3D morphology of Zn electrode after 50 cycles with various electrolytes (e) without DOL, and (f) with 100mM DOL. (g) Average surface thickness comparison of laser microscopes after different electrolyte cycles. (h) Comparison of XRD pattern after cycling of different electrolytes. (i) Plot of electrochemical properties of the present work compared with data from other literatures.

The influence of DOL on zinc deposition behavior was visualized through *in-situ* optical microscopy observations of Zn//Zn symmetric cells over a 1-hour period. In the pristine electrolyte, dendrite formation was observed initiating at the electrode edges and becoming increasingly pronounced over time (Figure

4a). In contrast, the 100 mM DOL-modified electrolyte exhibited uniform and stable deposition without visible dendrite formation throughout the charging-discharging process (Figure 4c).[50] Detailed morphological characterization of zinc deposits was conducted using multiple microscopy techniques. *Ex-situ* scanning electron microscopy (SEM) analysis revealed distinct surface topographies. The 100 mM DOL-modified electrolyte produced notably planar deposits (Figure 4d), whereas both the pristine and low-DOL-concentration electrolytes resulted in irregular, rough surface morphologies (Figure 4b, S14).[51,52] Further morphological investigation using confocal laser scanning microscopy (CLSM) provided comprehensive surface analysis through optical and height mapping (Figure S15). Three-dimensional imaging demonstrated significantly smoother surface topology with 100 mM DOL addition, contrasting with pronounced peak-like projections observed in the pristine electrolyte (Figure 4e-f). Quantitative height analysis revealed that DOL-modified deposits exhibited substantially reduced surface thickness (1.851 μm) compared to deposits from the pristine electrolyte (3.216 μm) (Figure 4g). This multi-technique microscopic characterization conclusively demonstrates DOL's regulatory effect on zinc deposition behavior, promoting uniform deposition that enhances cycling stability and longevity.[34] Furthermore, The XRD patterns were collected using Cu Kα radiation (λ = 1.5418 Å) at a scanning rate of 15° min^{-1} over the 2θ range of 3-90°. The diffraction peaks at 2θ=36.292°, 38.992° and 43.231°, Corresponding to the (002), (100), (101) crystal faces of zinc foil (PDF#04-0831), while the novel diffraction peak at 7.309° corresponding is linked to the by-product ZHS. XRD analysis of varying DOL concentrations after 50 hours of cycling revealed that 100 mM DOL exhibited the lowest ZHS peak intensity (Figure S16, 4h), indicating minimal by-product formation on the zinc surface. Time-dependent studies further demonstrated that the DOL-modified system maintained consistently low by-product levels from 20 to 60 cycles, whereas the pristine electrolyte showed persistently high by-product peaks (Figure S17).[53] In order to explore whether DOL can be adsorbed on the surface of zinc foil for a long time to regulate deposition behavior, FT-IR analysis was carried out on the recycled cells. The results showed that after 200 cycles, zinc foil with DOL added had a strong absorption peak at 620.81 cm^{-1}, which is speculated to be caused by bending vibration of -CH. In addition, it is found that the peak strength of -OH stretching vibration at 3000cm^{-1} is enhanced and redshift occurs, which is due to the interaction between DOL adsorbed on the zinc foil surface and the electrolyte (Figure S18).[54] In addition, to further confirm, we also performed XPS analysis of the zinc foil after circulation. The C 1s peak can be decomposed into C=O, C-O, -C-C-/C-H bonds. The results show that the proportion of C-O oxygen bonds with DOL added is significantly higher than that without DOL added, which is attributed to the adsorption of -C-OH groups in DOL on the surface of zinc foil. Then we analyzed O 1s. The results show that the C-O bond ratio of zinc foil with DOL is also higher than that of zinc foil without DOL, which confirms that DOL can preferentially adsorb on the surface of zinc foil and prevent it from side reactions. Similarly, we found that the binding energy of zinc foil Zn 2p supplemented with DOL was slightly increased, which we speculated was the result of DOL improving the coordination environment of Zn^{2+} and decreasing the active water molecules(Figure S19).[55] Comparative studies demonstrated DOL's superior performance enhancement relative to other electrolyte additives (Figure 4j).[28,29,31,35,36,40,56,57] Full-cell testing revealed higher capacity retention and initial specific capacity compared to previous reports (Table S2). The exceptional performance of DOL can be attributed to its hydrophilic polyhydroxyl groups, which preferentially adsorb zinc, modify the zinc deposition process, and reshape the Zn^{2+} solvation sheath. Furthermore, the hydrogen bonding between DOL's hydroxyl groups and water molecules reduces free water content, simultaneously suppressing side reactions (such as HER) and potentially enhancing low-temperature performance.

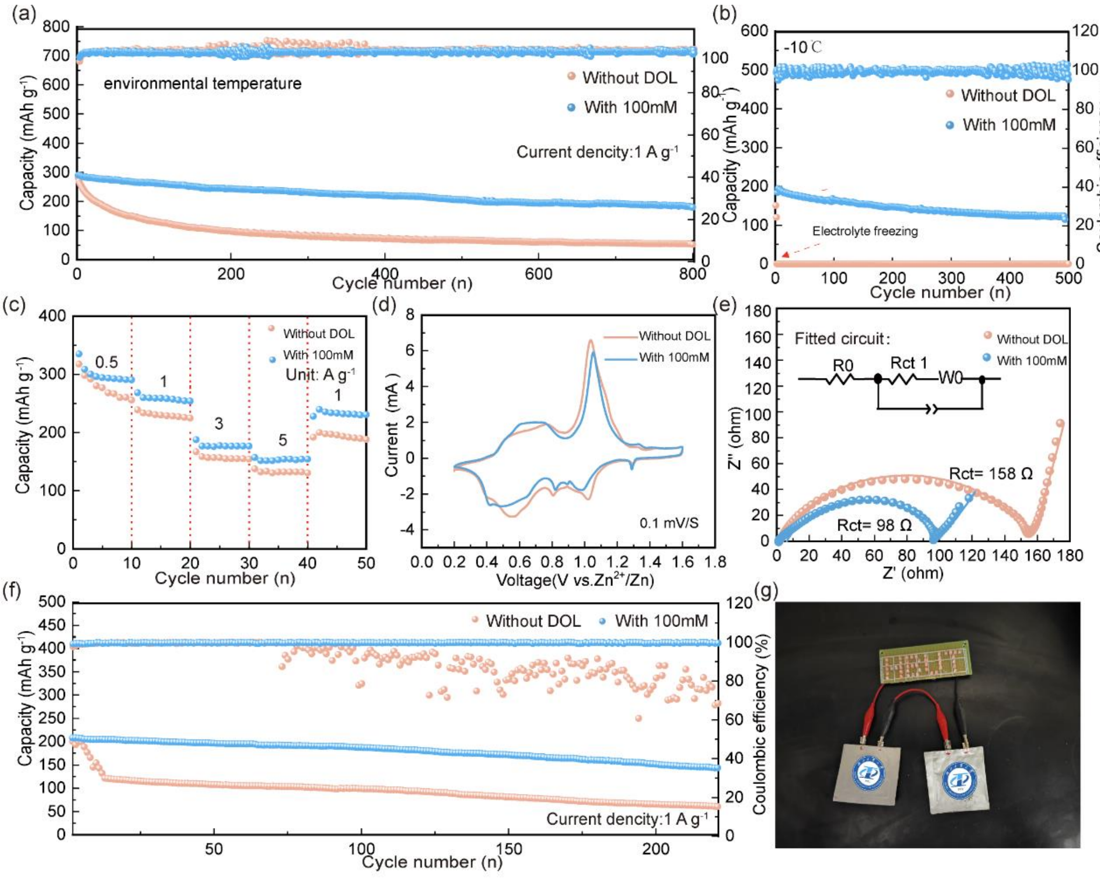

Figure 5. Different electrolytes assembled NVO//Zn full cell performances. (a) Long-cycle performance of NVO//Zn full cell with a current density of 1 A g^{-1} at room temperature. (b) Long-cycle performance

of NVO //Zn full cell with a current density of 1 A g^{-1} at -10 °C. (c) Rate performance of NVO//Zn full cells at current densities of 0.5 to 5 A g^{-1}. (d) CV curves of NVO//Zn full cells at a scan rate of 0.1 mV S^{-1}. (e) EIS curves for NVO//Zn full cells with different electrolytes. (f) Long cycle performance of NVO//Zn soft pack batteries at 1 A g^{-1}. (g) NVO//Zn soft pack batteries in series to illuminate the light.

The practical efficacy of DOL additives was systematically evaluated using NVO cathode material, synthesized via a one-step hydrothermal method (Figure S20) and confirmed by XRD analysis to match the standard pattern (PDF#31-0075) (Figure S21). NVO//Zn full cells were assembled with varying DOL concentrations in the electrolyte and subjected to long-term cycling tests at 1 A g^{-1}. After 800 cycles, cells containing 100 mM DOL maintained a stable capacity of 183.07 mAh g^{-1} with minimal fluctuation in the capacity retention curve. In contrast, DOL-free cells exhibited severe capacity fading, declining from an initial capacity of 297.10 mAh g^{-1} to merely 46.2 mAh g^{-1} (Figure 5a). Low-temperature cycling performance of NVO//Zn full cells was evaluated at -10 °C. Remarkably, cells with 100 mM DOL demonstrated exceptional stability at this extreme temperature, maintaining a high specific capacity of 155.95 mAh g^{-1} over 600 cycles with CE consistently approaching 100%. In contrast, DOL-free cells experienced rapid electrolyte freezing under these conditions, resulting in complete capacity loss (0 mAh g^{-1}) within merely 5 cycles (Figure 5b). Galvanostatic charge-discharge (GCD) profiles were recorded at various cycle intervals to facilitate detailed electrochemical analysis (Figure S22). Rate capability tests conducted across current densities ranging from 0.5 to 5 A g^{-1} demonstrated that DOL-modified cells consistently delivered superior capacity retention compared to their DOL-free counterparts at all tested rates (Figure 5c). The significant performance enhancement by DOL was consistently demonstrated in full-cell configurations. To elucidate the underlying mechanisms responsible for this superior performance, comprehensive electrochemical characterization was conducted on the assembled cells. The CV curves measured at 0.1 mV s^{-1} reveal that the addition of DOL leads to decreased redox peak intensities, indicating modified reaction kinetics. This observation aligns with our activation energy calculations showing reduced energy barriers in DOL-containing electrolyte. The decreased peak intensities can be attributed to the DOL molecules partially replacing water in the Zn^{2+} solvation shell, which weakens the Zn^{2+}-solvent interaction and facilitates the desolvation process. This enhanced charge transfer kinetics, combined with the stabilized interface structure, contributes to the improved electrochemical performance, as evidenced by the excellent capacity retention at both room temperature and -10°C (Figure 5d). [58] Subsequently, EIS analysis revealed significantly lower impedance in DOL-modified cells compared to DOL-free cells (98 Ω *vs*. 158 Ω), indicating enhanced charge transfer kinetics and improved material diffusion (Figure 5e).[59] To evaluate practical applicability, DOL-based electrolytes were tested in soft-pack battery configurations. The results demonstrated that DOL effectively stabilized the anode interface, enabling sustained capacity retention of 165 mAh g^{-1} with exceptional CE over 250 cycles, markedly outperforming DOL-free cells (Figure 5f). Further validation under high-loading conditions showed that DOL-modified NVO//Zn cells maintained a robust capacity of 292 mAh g^{-1} after 300 cycles. In contrast, DOL-free cells exhibited severe capacity degradation under identical conditions, declining from 360 to 144 mAh g^{-1} within the same cycling period (Figure S23).[60] These comprehensive results across various testing conditions conclusively demonstrate DOL's significant potential as an effective electrolyte additive for practical AZIB applications.

3. Conclusion

To summary, the introduction of 100 mM DOL as an additive in the conventional $ZnSO_4$ electrolyte significantly enhance the Zn anode stability. The hydrogen-bond-rich DOL effectively reconstructs the electrolyte's hydrogen bonding network, resulting in reduced desolvation energy barriers and enhanced Zn^{2+} transport numbers. This modification optimizes Zn^{2+} coordination by partially replacing water molecules, thereby reducing reactive water content and suppressing parasitic reactions at the Zn anode. the polyhydroxylated structure of DOL exhibits preferential adsorption on the Zn anode surface compared to H_2O molecules, promoting uniform Zn deposition and effectively suppressing dendrite formation. Furthermore, DOL molecules facilitate the conversion of free-water to bound-water, significantly lowering the electrolyte's freezing point. Attributing to these advantages, DOL-modified electrolytes enabled remarkable electrochemical performance. The Zn//Zn symmetric cells achieved stable cycling for 2000 h at 2 mA cm^{-2} and 1 mAh cm^{-2}, while NVO //Zn full cells maintained a high capacity of 183.07 mAh g^{-1} with 63 % retention after 800 cycles at 1 A g^{-1}. Moreover, DOL molecules promoted the conversion of free-water to bound-water, effectively lowering the electrolyte's freezing point. This enhancement enabled NVO//Zn full cells to retain 155.95 mAh g^{-1} capacity after 600 cycles even at -10°C. The successful implementation of DOL as an electrolyte additive establishes a promising strategy for developing low-temperature-tolerant AZIBs.

4. Experimental Section

4.1 Materials preparation

Electrolyte preparation：The fixed concentration of 2 M $ZnSO_4$ solution was prepared by add 3.2294 g zinc sulfate ($ZnSO_4$ Macklin 92 %) into 10 ml deionized water and obtained $ZnSO_4$ electrolyte. To the prepared 10 ml of $ZnSO_4$ electrolyte 0.0364 g, 0.18217 g, 0.3643 g and 0.722828 g of Dulcitol (DOL) ($C_6H_{14}O_6$ Macklin) was added to obtain $ZnSO_4$/DOL mixed electrolyte. The optimized concentration of Dulcitol is 0.3643 g and the corresponding electrolyte is denoted as 100 mM DOL.

Anode preparation：The zinc anodes used in the experiments were all circular pieces with a diameter of 12 mm. The zinc foils were ultrasonically cleaned using anhydrous ethanol for 10 minutes and then dried in an oven at 60°C for 12 hours.

Cathode preparation : The NVO powder synthesis method: One-step hydrothermal synthesis of NVO powder. More specifically, add 1.17 g of ammonium metavanadate (NH_4VO_3, Adamas, 99 %) to 70 ml of DI water and stir until thoroughly dissolved. Then 1.891 g of oxalic acid dihydrate ($H_2C_2O_4 \cdot 2H_2O$, SCRC, 99 %) was added into the solution and stirred at room temperature until the solution changed color. The mixed solution was transferred to Teflon-lined autoclave and heated at 140 °C for 720 min. After the reaction was completed, the NVO powder was washed with DI and dried at 70 °C for 720 min.

NVO powder was firstly mixed with carbon black (C Aladdin 99.5%), polyvinylidene fluoride (PVDF) in a weight ratio of 7:2:1 and using 1-Methyl-2-pyrrolidinone (NMP Aladdin AR>99%) as solvent. The configured slurry was uniformly coated on the hydrophilic carbon cloth and dried at 60°C for 12 h before using, which was cut into discs with a diameter of 10 mm as cathodes. The loading of the NVO cathode was controlled to be about 2~3 mg cm $^{-2}$, and the additives were added to be 100 μL each time.

4.2 Battery assembly

All CR2032 coin cells were made with 19 mm diameter separators (Whatman GF/A), and cells with different electrodes and electrolytes were assembled at room temperature (25°C). Specifically, The Zn//Zn symmetric cell is an assembly of two zinc foils that serve as the cathode and anode, respectively. And the full cell was NVO as cathode (cathode preparation as described above), with a loading of 2~3 mg cm^{-2} per cathode, and the zinc foils served as anodes. Each time the cell was assembled 100 μL of electrolyte was added dropwise. The CE of Zn//Cu half-cells with different electrolytes were compared at a current density of 2 mA cm^{-2} area capacity of 1 mA cm^{-2} and a cut-off voltage of 0.8 V.

4.3 Materials characterization

The contact angles between different electrolytes and Zn electrode were measured by using

Dataphysics OCA 20 (German) with 5 μL of electrolyte for each test. The ^{1}H NMR (Bruker 400MHz) was performed on the different electrolytes by taking an appropriate amount of sample (about 10 mg) in a 1500 μL centrifuge tube and then adding 500 μL D_2O. After completely dissolved, the solution was transferred into the NMR tube through a pipette gun and measured. The FT-IR results were acquired by the Thermo Scientific Nicolet iS20 (American). In a dry environment, the ATR accessory is placed in the optical path of the spectrometer, the air background is scanned, and 5 μL of liquid is applied to the crystal surface of the ATR accessory with a dropper, and then the infrared spectrum of the sample is collected with a resolution of 4 cm^{-1}, a number of scans of 32, and a range of test wave numbers from 400~4000 cm$^{-1.}$ Furthermore, the Raman spectra were measured by the HORIBA Scientific LabRAM HR Evolution (Japan, λ = 532 nm). The *in-situ* optical microscope was conducted on RIEVBCAU MS4. The morphology of zinc foil before and after electrochemical cycling in different electrolytes was obtained by scanning electron microscope (SEM, JSM-6390LV). Confocal laser scanning microscope (CLSM) experimental images were obtained from KEYENCE VK-X150, KEYENCE VK-X1000.The XRD patterns were obtained by Rigaku SmartLab 3KW X-ray diffractometer (Japan) and Cu Kα radiation in the 2θ range of 3° to 90° at 15° min^{-1}.

4.4 Electrochemical measurements

All electrochemical measurement dates collected via the CHI660E and Corrtest electrochemical workstation. The CA was conducted with an overpotential of -150 mV within 400 s. Nucleation overpotential of Zn//Ti half-symmetric cell measured by CV tested with a scan range from -0.3 to 1.0 V and a scan rate of 10 mV S^{-1}. The Tafel plots curve of electrolyte were measured with three-electrode system, with Zn foil as the work electrode, Pt foil as the counter electrode, and Ag/AgCl as the reference electrode. The test range was -1.3 to -0.7 V with a sweep rate of 1 mV S^{-1}. The S curves of NVO//Zn full cells was measured with a scan range of 0.2-1.6 V and a scan rate of 1 mV S^{-1}. EIS of all samples were measured using CR2032 coin cells within a frequence range between 0.01 Hz and 100000 Hz at a constant temperature.

Acknowledgements

This work was funded by the Startup fund at Hubei University of Technology, and High-level talent grant of Hubei province.

Conflicts of interest

The authors declare no conflict of interest.

References

[1] P. K. Nayak, L. Yang, W. Brehm, P. Adelhelm, *Angewandte Chemie - International Edition* **2018**, *57*, 102.

[2] X. Wang, G. Tan, Y. Bai, F. Wu, C. Wu, *Multi-Electron Reaction Materials for High-Energy-Density Secondary Batteries: Current Status and Prospective*, Springer Singapore, **2021**.

[3] Q. Wang, J. Xu, W. Zhang, M. Mao, Z. Wei, L. Wang, C. Cui, Y. Zhu, J. Ma, *J Mater Chem A Mater* **2018**, *6*, 8815.

[4] Q. Liu, H. Wang, C. Jiang, Y. Tang, *Energy Storage Mater* **2019**, *23*, 566.

[5] Y. Li, Z. Wang, Y. Cai, M. E. Pam, Y. Yang, D. Zhang, Y. Wang, S. Huang, *Energy and Environmental Materials* **2022**, *5*, 823.

[6] M. Li, Z. Li, X. Wang, J. Meng, X. Liu, B. Wu, C. Han, L. Mai, *Energy Environ Sci* **2021**, *14*, 3796.

[7] S. Islam, S. Ul, A. Shibly, S. Iffat, Nanomaterials **2022**, 12(22) ,1-26.

[8] F. Wan, Z. Niu, *Angewandte Chemie* **2019**, *131*, 16508.

[9] X. Gao, Y. Dai, C. Zhang, Y. Zhang, W. Zong, W. Zhang, R. Chen, J. Zhu, X. Hu, M. Wang, R. Chen, Z. Du, F. Guo, H. Dong, Y. Liu, H. He, S. Zhao, F. Zhao, J. Li, I. P. Parkin, C. J. Carmalt, G. He, *Angewandte Chemie - International Edition* **2023**, *62*, DOI 10.1002/anie.202300608.

[10] Y. Shang, D. Kundu, *Batter Supercaps* **2022**, *5*, DOI 10.1002/batt.202100394.

[11] X. Jia, C. Liu, Z. G. Neale, J. Yang, G. Cao, *Chem Rev* **2020**, *120*, 7795.

[12] R. Chen, W. Zhang, Q. Huang, C. Guan, W. Zong, Y. Dai, Z. Du, Z. Zhang, J. Li, F. Guo, X. Gao, H. Dong, J. Zhu, X. Wang, G. He, *Nanomicro Lett* **2023**, *15*, 81.

[13] Q. Chen, K. Ouyang, Y. Wang, M. Chen, H. Mi, J. Chen, C. He, H. Li, D. Ma, P. Zhang, *Adv Funct Mater* **2024**, *2406386*, 1.

[14] D. Wang, Q. Li, Y. Zhao, H. Hong, H. Li, Z. Huang, G. Liang, Q. Yang, C. Zhi, *Adv Energy Mater* **2022**, *12*, DOI 10.1002/aenm.202102707.

[15] G. Fang, J. Zhou, A. Pan, S. Liang, *ACS Energy Lett* **2018**, *3*, 2480.

[16] D. Chen, M. Lu, D. Cai, H. Yang, W. Han, *Journal of Energy Chemistry* **2021**, *54*, 712.

[17] P. Sun, L. Ma, W. Zhou, M. Qiu, Z. Wang, D. Chao, W. Mai, *Angewandte Chemie* **2021**, *133*, 18395.

[18] A. Wang, W. Zhou, A. Huang, M. Chen, Q. Tian, J. Chen, *J Colloid Interface Sci* **2021**, *586*, 362.

[19] H. Ren, S. Li, B. Wang, Y. Gong, H. Zhang, J. Wang, Q. Lv, D. Wang, H. Liu, S. Dou, *Energy Storage Mater* **2024**, *68*, DOI 10.1016/j.ensm.2024.103364.

[20] J. Shin, J. Lee, Y. Park, J. W. Choi, *Chem Sci* **2020**, *11*, 2028.

[21] T. Zhou, L. Zhu, L. Xie, Q. Han, X. Yang, L. Chen, G. Wang, X. Cao, *J Colloid Interface Sci* **2022**, *605*, 828.

[22] Q. Deng, S. You, W. Min, Y. Xu, W. Lin, J. Lu, C. Yang, *Advanced Materials* **2024**, *36*, 16,2312924.

[23] H. Li, L. Yang, S. Zhou, J. Li, Y. Chen, X. Meng, D. Xu, C. Han, H. Duan, A. Pan, *Adv Funct Mater* **2024**, *34*, 19,2313859.

[24] X. Zhang, L. Chen, R. Orenstein, X. Lu, C. Wang, M. Yanilmaz, M. Peng, Y. Dong, Y. Liu, X. Zhang, *Energy Storage Mater* **2024**, *70*, 103500.

[25] Q. Gou, H. Luo, Q. Zhang, J. Deng, R. Zhao, O. Odunmbaku, L. Wang, L. Li, Y. Zheng, J. Li, D. Chao, M. Li, *Small* **2023**, *19*, DOI 10.1002/smll.202207502.

[26] Y. Huang, Y. Zhuang, L. Guo, C. Lei, Y. Jiang, Z. Liu, Y. Zhao, K. Xing, X. Wu, S. Luo, G. Chen, Z. Liu, Z. Hu, *Small* **2024**, *20*, 10,2306211.

[27] Z. Li, Y. Li, X. Ren, Y. Zhao, Z. Ren, Z. Yao, W. Zhang, H. Xu, Z. Wang, N. Zhang, Y. Gu, X. Li, D. Zhu, J. Zou, *Small* **2023**, *19*, DOI 10.1002/smll.202301770.

[28] D. Xie, Y. Sang, D. H. Wang, W. Y. Diao, F. Y. Tao, C. Liu, J. W. Wang, H. Z. Sun, J. P. Zhang, X. L. Wu, *Angewandte Chemie - International Edition* **2023**, *62*, DOI 10.1002/anie.202216934.

[29] Q. Zong, Y. Yu, C. Liu, Q. Kang, B. Lv, D. Tao, J. Zhang, J. Wang, Q. Zhang, G. Cao, *Chemical Engineering Journal* **2024**, *479*, DOI 10.1016/j.cej.2023.147759.

[30] Z. Zhao, C. Tang, Y. Zhang, H. Zhang, X. Shi, H. Zhao, G. Wang, J. Liu, L. Li, *Energy Storage Mater* **2024**, *70*, 103515.

[31] W. Ding, G. Zhou, X. Guo, C. Liu, T. Wang, Y. Fu, J. Yin, L. Zhang, E. H. Ang, *Chemical Engineering Journal* **2024**, *481*, 148544.

[32] J. Luo, L. Xu, Y. Zhou, T. Yan, Y. Shao, D. Yang, L. Zhang, Z. Xia, T. Wang, L. Zhang, T. Cheng, Y. Shao, *Angewandte Chemie* **2023**, *135*, DOI 10.1002/ange.202302302.

[33] R. Wang, S. Xin, D. Chao, Z. Liu, J. Wan, P. Xiong, Q. Luo, K. Hua, J. Hao, C. Zhang, *Adv Funct Mater* **2022**, *32*, 51,2207751.

[34] T. Wei, X. Zhang, Y. Ren, Y. Wang, Z. Li, H. Zhang, L. Hu, *Chemical Engineering Journal* **2023**, *457*, 141272.

[35] Y. Quan, M. Yang, M. Chen, W. Zhou, X. Han, J. Chen, B. Liu, S. Shi, P. Zhang, *Chemical Engineering Journal* **2023**, *458*, 141392.

[36] Z. Wang, Z. Hu, M. Ye, J. Chen, Y. Chen, Z. Wen, Y. Zhang, Y. Tang, X. Liu, C. C. Li, *Chemical Engineering Journal* **2024**, *481*, DOI 10.1016/j.cej.2023.148511.

[37] Y. Xiong, X. Gu, Z. Liu, X. Ren, Y. Jiang, H. Xu, L. Zhuo, G. Jiang, *J Colloid Interface Sci* **2024**, *662*, 604.

[38] J. Wan, R. Wang, Z. Liu, L. Zhang, F. Liang, T. Zhou, S. Zhang, L. Zhang, Q. Lu, C. Zhang, Z. Guo, *ACS Nano* **2022**, DOI 10.1021/acsnano.2c11357.

[39] Q. Zhang, Y. Ma, Y. Lu, L. Li, F. Wan, K. Zhang, J. Chen, *Nat Commun* **2020**, *11*, 4463.

[40] Z. Liu, R. Wang, Q. Ma, J. Wan, S. Zhang, L. Zhang, H. Li, Q. Luo, J. Wu, T. Zhou, J. Mao, L. Zhang, C. Zhang, Z. Guo, *Adv Funct Mater* **2024**, *34*, 5,2214538.

[41] T. Fang, Q. Liu, A. Hu, J. Meng, Y. Fu, Z. Shi, *J Power Sources* **2023**, *581*, 233521.

[42] Z. Chen, J. Feng, P. Yao, J. Cai, W. Zhou, J. Lu, L. Zhang, L. Sheng, H. Gu, F. R. Wang, Z. Hao, *Electrochim Acta* **2024**, *508*, 145291.

[43] Y. Quan, M. Yang, M. Chen, W. Zhou, X. Han, J. Chen, B. Liu, S. Shi, P. Zhang, *Chemical Engineering Journal* **2023**, *458*, DOI 10.1016/j.cej.2023.141392.

[44] D. Zhang, J. Cao, Z. Dai, R. Chanajaree, C. Yang, X. Wu, X. Zhang, J. Qin, *J Mater Chem A Mater* **2023**, *11*, 23779.

[45] Q. Zhao, W. Liu, X. Ni, H. Yu, C. Zhang, B. Wang, L. Jiang, H. He, Y. Chen, L. Chen, *Adv Funct Mater* **2024**,34,41, *2404219*,.

[46] Q. Qiu, X. Chi, J. Huang, Y. Du, Y. Liu, *ChemElectroChem* **2021**, *8*, 858.

[47] Q. Zhang, X. Gao, K. Liu, N. Gao, S. Cheng, Y. Dai, H. Dong, J. Liu, G. He, H. Li, *Commun Chem* **2024**, 173.

[48] T. Wei, Y. Peng, L. Mo, S. Chen, R. Ghadari, Z. Li, L. Hu, *Sci China Mater* **2022**, *65*, 1156.

[49] Q. Guan, J. Li, L. Li, P. Chai, Y. Li, S. Zhang, X. Yu, L. Bao, J. Peng, X. Li, *Chemical Engineering Journal* **2023**, *476*, 146534.

[50] J. Wan, R. Wang, Z. Liu, L. Zhang, F. Liang, T. Zhou, S. Zhang, L. Zhang, Q. Lu, C. Zhang, Z. Guo, *ACS Nano* **2023**, *17*, 1610.

[51] Z. Liu, R. Wang, Y. Gao, S. Zhang, J. Wan, J. Mao, L. Zhang, H. Li, J. Hao, G. Li, L. Zhang, C.

Zhang, *Adv Funct Mater* **2023**, *33*, 49,2308463.

[52] W. Zhou, M. Chen, Y. Quan, J. Ding, H. Cheng, X. Han, J. Chen, B. Liu, S. Shi, X. Xu, *Chemical Engineering Journal* **2023**, *457*, 141328.

[53] H. Huang, D. Xie, J. Zhao, P. Rao, W. M. Choi, K. Davey, J. Mao, *Adv Energy Mater* **2022**, *12*, DOI 10.1002/aenm.202202419.

[54] T. B. Song, Z. H. Huang, X. R. Zhang, J. W. Ni, H. M. Xiong, *Small* **2023**, *19*, DOI 10.1002/smll.202205558.

[55] W. Lv, Y. Tan, C. Guo, X. He, L. Zeng, J. Zhu, L. Yang, Z. Chen, X. Yin, J. Xu, H. He, *Adv Energy Mater* **2024**, *2403689*.

[56] S. Wang, Z. Wang, B. He, S. Yuan, Z. Wang, Y. Liu, J. Xin, X. Zhou, H. J. Fan, L. Wei, *Nano Energy* **2024**, *126*, 109661.

[57] J. Cao, D. Zhang, R. Chanajaree, Y. Yue, Z. Zeng, X. Zhang, J. Qin, *Advanced Powder Materials* **2022**, *1*, 100007.

[58] S. J. Zhang, J. Hao, D. Luo, P. F. Zhang, B. Zhang, K. Davey, Z. Lin, S. Z. Qiao, *Adv Energy Mater* **2021**, *11*, 37,2102010.

[59] W. Zhang, Y. Dai, R. Chen, Z. Xu, J. Li, W. Zong, H. Li, Z. Li, Z. Zhang, J. Zhu, F. Guo, X. Gao, Z. Du, J. Chen, T. Wang, G. He, I. P. Parkin, *Angewandte Chemie - International Edition* **2023**, *62*, DOI 10.1002/anie.202212695.

[60] X. Guo, Z. Zhang, J. Li, N. Luo, G. L. Chai, T. S. Miller, F. Lai, P. Shearing, D. J. L. Brett, D. Han, Z. Weng, G. He, I. P. Parkin, *ACS Energy Lett* **2021**, *6*, 395.